Study of concentric, eccentric and split type magnetic membrane micro-mixers

Author

Tang, SQ, Li, KHH, Yeo, ZT, Chan, WX, Tan, SH, Yoon, YJ, Ng, SH

Published

2018

Journal Title

Sensing and Bio-Sensing Research

Version

Accepted Manuscript (AM)

DOI

10.1016/j.sbsr.2018.04.001

ABSTRACT

Electromagnetically driven elastic magnetic microfluidic mixers were investigated for their performance in air, water and glycerol filled chambers. They were fabricated by embedding flexible magnets in polydimethylsiloxane (PDMS) membrane. At a driving frequency of 100 Hz, oscillating fluid flow was induced and mixing was achieved.. Three designs were fabricated and studied: a) concentric type with the magnetic material in the center of the membrane, b) eccentric type with the magnetic material offset from the center of the membrane and c) split type with two regions of magnetic materials with opposing polarities. The split configuration provides additional fluid folding, facilitating mixing of the 20 µL fluorescent dye in 60 µL of solvent. Simulation and experimental results show that the eccentric and split designs were able to achieve a 20-30 % reduction in mixing time compared to the concentric design. At the same magnetic flux density, the eccentric type design exhibited the greatest deflection, explaining the better mixing achieved over the concentric type design. The split type design, having the lowest deflection, was able to perform better and more consistently than the eccentric type design by creating a "micro rocker mixer" effect. We postulated that the shapes of the deflection profiles in the eccentric and split designs contributed to the mixing efficiency by promoting better chaotic advection than the concentric design.

1. Introduction

Microfluidic technology has generated significant interest over the past few years due to the inherent advantages in terms of small volume, response time and cost reduction. This trend is evident based on the increasing number of articles and patents published yearly [1]. An example of a successful microfluidic system application is the handheld patient-side blood testing device [2]. Such devices require mixing of fluids to obtain diagnostic test results, which allow healthcare professionals to make an accurate treatment decision [2]. However, due to the very low Reynolds number (from less than 1 to 10) [3, 4, 31] and omnipresence of laminar flow in microfluidics, fluids can only be mixed through convection and molecular diffusion. This often requires a long period of time (which is in one order magnitude) [31] to achieve complete mixing [3]. Hence, it is apparent that an efficient micro-mixer is needed for such applications. Typically, in microfluidics channels, the diffusion time is on the order of magnitude of 1 for 100 um of diffusion distance, as estimated with the relation – $T = L^2/D$, where L is the diffusion distance and D is the diffusion coefficient for the solute in the fluid [30, 31]. For example, the diffusion of sucrose in water over a distance of 100 um, would occur in 20 s, given the diffusion coefficient of sucrose in water to be about 0.5×10^{-9} m^2/s [44]. Considering a typical flow rate of around 100 mm/s, adjacent streams of different fluids should flow over distances of 200 cm or more before mixing of sucrose is completed via diffusion. This constraint is undesirable for the miniaturization of the microfluidics devices. On the other hand, complex structures such as grooves and ribs [33, 39-43] can be used to enhance mixing in passive micro-mixer. However, these structures are often complex in designs which increases the difficulty in the fabrication of the devices.

Hence, chaotic, advection-based active micro-mixers are often preferred over passive micro-mixer. Among the advection-based micro-mixers are the T-junction mixers. Researchers have shown that, with the use of oscillating flows confluent at a T-junction, the mixing lengths can be significantly reduced by 2 orders of magnitude, as compared to that required for passive mixing - from tens of centimeters to millimeters [28]. Also, Okkela and Tabeling have shown numerically and experimentally that violent folding of streams occur at a T-junction when the amplitude of flow disturbance normalized against the velocity of flow is greater than the product of the Strouhal number with 2π [29]. Spatial-temporal resonances of a folding quantity have been plotted by Okkels and Tabeling, relating a series of amplitude of flow disturbances and Strouhal number combinations at which folding of the fluid flows is maximized. For an open flow system, the T-junction mixers are unsuitable as the mixing activity is being limited to the dimensions of the junction. A long downstream channel is still required for mixing to be completed passively after the phase-to-phase interface has been stretched. Hence, in this paper, an oscillating flow is applied in a closed environment, such as in a temporarily isolated chamber, to complete the fluids mixing before channeling the mixed fluids to other segments of the lab-on-chip devices. This reduces the overall footprint of the micro-mixer required.

There are various methods to generate an oscillating flow field. One of which, is to use magnetically driven actuators which are able to provide robust and wireless operations. These actuators are ideal in miniaturized applications [7] and could potentially be applied to several applications in microfluidics. The use of magnetic membranes was reported in many works, demonstrating various actuation purposes [8], in the form of an elastomer with permanent magnets attached or embedded within [9] or by introducing nano-sized magnetic particles into the polymer matrix [10], which may be structured as a micropillar [11]. However, the implementation of permanent magnets into microsystems may result in cracking and face poor adhesion with the substrate which could affect the performance of the micro-mixers. Furthermore, this is often limited to the size and shape of permanent magnets available commercially. Introduction of magnetic nanoparticles into polymer may result in undesired agglomeration, thus affecting polymer elasticity and performance. Such magnetic composite polymers are also not able to produce large deflection, limiting the efficiency

of mixing and requiring longer duration to complete the mixing process. Chong et al. [15] did a brief study using a flexible magnet integrated with PDMS and demonstrated its potential of being a micro-mixer. In contrast to magnetic membranes containing ferromagnetic particles which could only be actuated by attractive forces, this flexible magnet could be actuated by both attractive and repulsive forces, with better response to an alternating external magnetic field.

In this study, three configurations with different magnetic cores were fabricated and studied. Specifically, two of the designs were able to create atypical shapes of the membrane profile via the innovative layouts of the magnetic cores. In one of the designs, we also demonstrated simultaneous attractive and repulsive actuation on a single membrane resulting in a different mixing effect. The effect of the magnetic field and the corresponding deflections to their performance in mixing were also studied. It is envisioned that such mixer configurations can be used in microtiter array plates to improve mixing.

2. Device design and fabrication

The magnetic core of the micro-mixer was cut from a flexible magnetic sheet (Eclipse Magnetics, 060510U10/W, 500 μm in thickness). This flexible magnetic core was then embedded into PDMS elastomer, forming a magnetic membrane to respond to electromagnetic field. The polarity of magnetization for the flexible magnetic sheets is usually arranged in a Halbach array [15] to concentrate the magnetic flux on one side of the sheet.

A gaussmeter with axial probe (Hirst, GM05 Gaussmeter) was used to measure along the flexible magnetic sheet to identify the width of each polarity zone which is about 3 mm wide(Figure 1). The boundaries between the positive and negative zones are mixed or neutral in terms of polarity. Multiple pieces of magnets were punched out with a 3 mm diameter puncher. Punching out at Location 1, for example, would give a predominating opposite polarity to Location 2, while Location 3 would give a mixed characteristic.

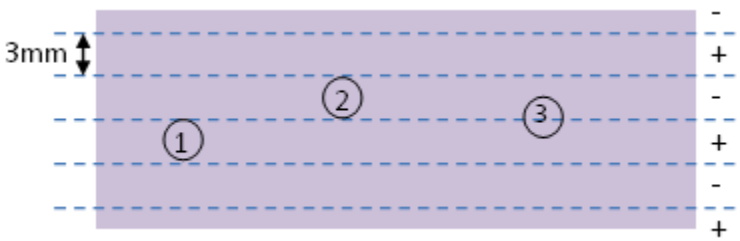

FIG. 1. Sample cut-out locations on Halbach array.

The fabrication process (Figure 2) of the mixer started with a spin coater (Laurell WS-400BZ-GNPP) where a layer of PDMS of about 25 μm in thickness was deposited on a PMMA wafer disc with a spin speed of 3200 rpm. The 3 mm diameter magnetic core was positioned on the first layer of PDMS, and the structure is partially cured before, a second layer of PDMS was spin-coated. After that, the PDMS was allowed to cure at 80 °C for 60 minutes [11]. This lower-than-typical curing temperature is chosen to achieve a greater flexibility of the PDMS membrane, with a Young's Modulus of around 1.8 MPa, as achieved also by Johnston et al [12]. This ensures sufficient displacement by the solenoid field, and effective mixing of fluid in the chamber. A typing curing temperature of around 125 °C would result in a Young's Modulus of 2.4 MPa [12], which would reduce the membrane deflection and resulting pressure on the fluid by 25 %. In addition, Johnston's group presented experimental data that shows that the time for the core of a 2 mm thick PDMS film to reach a curing temperature of 100 °C, is around 13 min or less. Since the PDMS layer of the magnetic membrane in our device is only 25μm or less, such a curing time of 60 min is sufficient for completely curing the PDMS at 80 °C. A similar curing

temperature is used by Fatemeh et. al. in fabricating a composite PDMS infused with iron oxide nanoparticles [13]. An open well was created by casting and curing a square slab of PDMS with a bore diameter of 6 mm. The magnetic membrane was then assembled to the PDMS well by plasma bonding (Plasma Cleaner PDC-32G) forming the mixing chamber.

Three designs were fabricated (Figure 3): a) concentric type with the magnetic paper/material in the centre of the membrane, b) eccentric type with the centre of the circular magnetic material offset by 1.5 mm from the centre of the membrane, and c) split type with the magnetic core consisting of two semicircles (radius 1.5 mm) with polarities in opposing directions, separated by a distance of 1.5 mm from each other and centred around the axis of the circular membrane. During perturbation by the solenoid field, the points of maximum displacement for the concentric and eccentric mixers are 0 mm and 1.5 mm from the centre of the circular membrane respectively. The points of maximum displacement for each of the opposite poles of the magnetic material, in the split mixer, are 2.25 mm from the centre of the membrane.

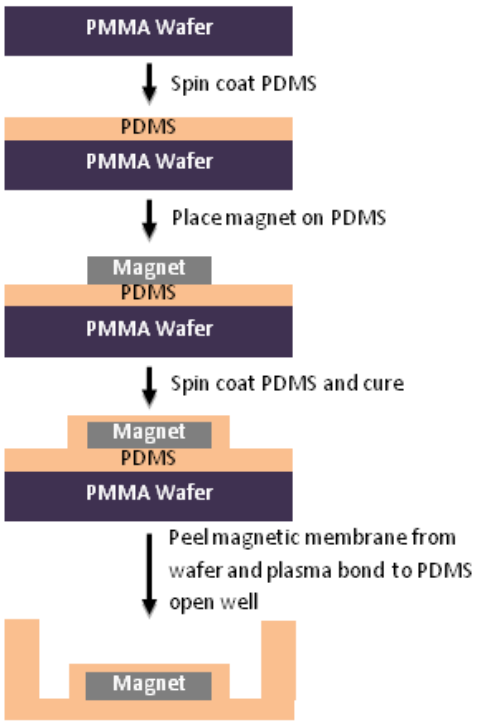

FIG. 2. Illustration of fabrication process.

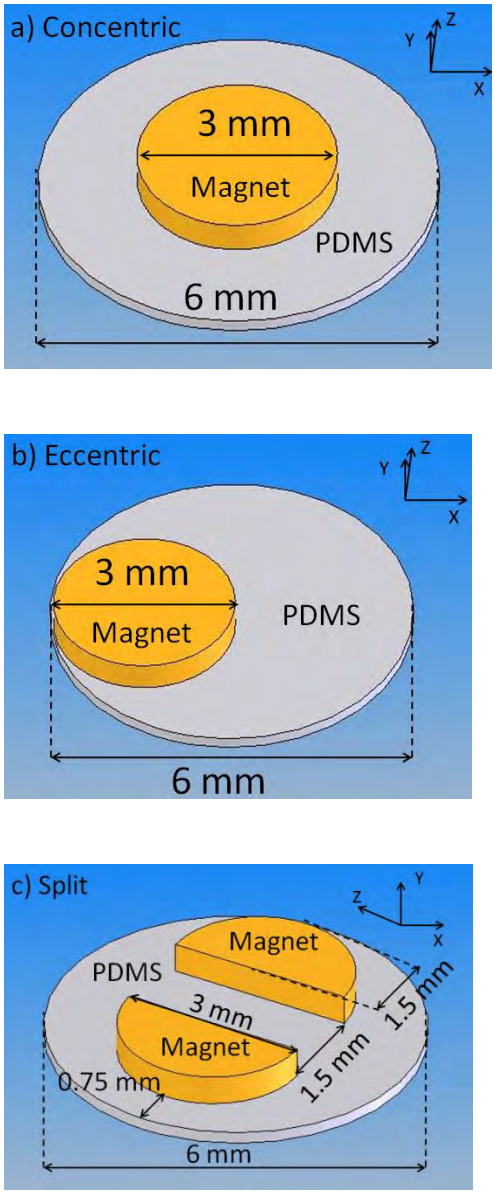

FIG. 3. Three designs of magnetic membrane: a) concentric type, b) eccentric type, c) split type (right).

3. Mathematical model of fluid flow during mixing

The full Navier Stokes Equation is used here, since strong advection flows are present.

$$\frac{d\vec{u}}{dt} + \vec{u}\nabla\vec{u} = -\frac{\text{grad}(p)}{\rho} + \left(\frac{\mu}{\rho}\nabla^2(\vec{u})^T\right) \qquad (1)$$

The dimensionless form of the above is obtained

$$\frac{d\vec{\tilde{u}}}{d\tilde{t}} + \vec{\tilde{u}}\tilde{\nabla}\vec{\tilde{u}} = -\text{grad}(\tilde{p}) + \frac{\tilde{\nabla}^2\left(\vec{\tilde{u}}\right)^T}{\text{Re}} \qquad (1a)$$

Where

$$\vec{\tilde{u}} = \frac{\vec{u}}{U}, \quad \tilde{p} = \frac{p}{\rho U^2}, \quad \tilde{\nabla} = \frac{\left(\partial_x \partial_y \partial_z\right)}{L}, \tilde{t} = \frac{t}{L/U}$$

And where

U: characteristic velocity of flow, being 1 ms^{-1}

ρ: density of fluid, being 1000 kgm^{-3} (for water)

L: the characteristic length scale, being 10^{-4} m (also the spatial step used in the discrete formulation)

μ: dynamic viscosity of fluid (0.001 Pas for water)

Re: Reynolds number given by $\mathrm{Re} = \frac{\rho UL}{\mu}$

The time-dependent component of the function can also assume a sine function, and from here, the time and space-dependent acceleration of each point of the membrane can be derived.

Assuming continuity of the bottom fluid layer with the membrane, starting with the displacement of the fluid layer immediately adjacent to the oscillating membrane, where F(x, z) is the two-dimensional spatial profile of the membrane deflection,

$$y = Y_0 F(x,z) \sin(\omega t) \tag{2}$$

the pressure imposed on the lowest layer of fluid adjacent to the oscillating membrane would be

$$p_m = \rho \ddot{y} = -\rho \omega^2 Y_0 F(x,z) \sin(\omega t) \tag{3}$$

The immediate layer of fluid above will experience, by Newton's 3nd Law,

$$p_f = -\rho \ddot{y} = \rho \omega^2 Y_0 F(x,z) \sin(\omega t) \tag{3a}$$

The dimensionless form of this would be

$$\tilde{p} = -\frac{\rho \ddot{y}}{\rho U^2} = \frac{\omega^2 Y_0}{U^2} F(x,z) \sin(\omega t) \tag{3b}$$

where

ω: angular frequency of oscillation of membrane displacement

x: Position along x-direction along plane of membrane

t: time

We define the pressure profile function, F(x, z) for the concentric mixer to be:

$$F_c(x,z) = \exp\left(-\frac{(x-x_c)^2 + (z-z_c)^2}{2\sigma_c^{\,2}}\right) \tag{4}$$

Where

x_c: is the position of the membrane with the highest deflection, centered in the plane of membrane

σ_c: the standard deviation of the Gaussian form(which is related to the width of the deflected membrane profile)

For the eccentric design, the pressure profile is described by the same form of expression, but with the position of the largest deflection, $x_e$and $z_e$set as a quarter of the diameter of the membrane.

$$F_e(x,z) = \exp\left(-\frac{(x-x_e)^2+(z-z_e)^2}{2{\sigma_e}^2}\right) \quad (5)$$

A realistic expression for the pressure imposed by split-mixer membrane could be composed of a pair of superposed anti-symmetric Gaussian functions:

$$F_s(x,z) = \exp\left(-\frac{(x-x_{s1})^2+(z-z_{s1})^2}{2{\sigma_s}^2}\right) - \exp\left(-\frac{(x-x_{s2})^2+(z-z_{s2})^2}{2{\sigma_s}^2}\right) \quad (6)$$

where

x_{s1}, z_{s1}:is the position of maximum deflection for the positive pole

x_{s2}, z_{s2} : is the position of maximum deflection for the negative pole

Subsequently, all tildes will be omitted from the dimensionless quantities, for convenience of expression.

Replacing F(x) with the appropriate form for the deflection profiles of each of the three mixers, we have, for the three designs, the pressure felt by the subsequent layer of fluid would be

$$\widetilde{p_c} = \frac{\omega^2 Y_0}{U^2}\sin(\omega t)\exp\left(-\frac{(x-x_c)^2+(z-z_c)^2}{2{\sigma_c}^2}\right) \quad \text{(Concentric)} \quad (7)$$

$$\widetilde{p_e} = \frac{\omega^2 Y_0}{U^2}\sin(\omega t)\exp\left(-\frac{(x-x_e)^2+(z-z_e)^2}{2{\sigma_e}^2}\right) \quad \text{(Eccentric)} \quad (8)$$

$$\widetilde{p_s} = \frac{\omega^2 Y_0}{U^2}\sin(\omega t)\left(\exp\left(-\frac{(x-x_{s1})^2+(z-z_{s1})^2}{2{\sigma_s}^2}\right) - \exp\left(-\frac{(x-x_{s2})^2+(z-z_{s2})^2}{2{\sigma_s}^2}\right)\right) \quad \text{(Split)} \quad (9)$$

4. Computational analysis of mixing performance

Various schemes were utilized for quantifying and visualizing the degree of stretching and folding of flow streamlines, including traditional methods of particle tracing for producing Poincare section maps of particle trajectories [19], a front-tracking technique by Galaktinov [20] and revisited by Anderson [21], and a mapping method of using distribution matrices for analyzing the mixing progress [22]. By tracking such three-

coordinate displacements of regularly marked initial elemental volumes in the fluid field, information about the mixing can be collected. Such is the case of the manifestation of the non-periodic orbits, which can be demarcated by the Kolmogorov-Aronold-Moser (KAM) curves, such that the flows within the KAM boundaries are regular and linear [21]. Lyapunov exponents, which are a measurement of the rate of exponential divergence of velocity over a particular time scale as time goes to infinity, are used as an indication of the onset of chaotic flow. Xize and Yi-Kuen have also independently found that the Lyapunov exponents, used as the mixing index, are closely related to the amplitude and stirring frequency [6]. It is also shown that in an oscillating flow generated by an oscillating lid, the amplitude of the lid velocity and Reynolds number, does not have an influence on the time at which the maximum Lyapunov exponent is reached, but a larger amplitude of lid velocity does result in a larger value of Lyapunov exponent, thereby increasing the rate of mixing in finite time [34]. They have also, in the same paper, proposed the use of the Lyapunov exponent as an indication of the rate of increase of the interface between the materials to be mixed, hence linking to the mixing performance.

Kusch, Ottino [24] and MetCalfe [25] attempted to relate the amount of stretching during the time of flow re-orientations. The Strouhal number, for an oscillating-transverse flow mixer at a T-junction, is found to be related to the target number of wavelengths of folded streams (half of the number of folds) that could develop within the width of the junction, measured parallel to the main channel flow. In the case of confined flows, as in the present invention, the Strouhal numbers consist of the projection of the flow velocity onto the axial direction of the vortex, and the frequency of oscillation is that of the transversal of the loops, as visualized in a Poincare section projection [21]. Nishimura and Kunitsuga [32] have done an extensive analysis of the velocity field in a cavity with an oscillating lid, resulting in a study of the vortex strength for different Strouhal number.

Whereas many studies, both theoretically and experimentally, have been done for the oscillating flat lid in a cavity mixer, our current work explores the mixing performance and fluid flow driven by an undulating surface with a non-uniform profile. It is envisaged that many interesting behaviors will arise out of the extra degrees of freedom offered by extra variation of the pressure divergence field. It is also observed in the experiments, that a sloshing effect [35] of the fluid, during the agitation of the membrane, leads to a feedback to the fluid flow field, leading to possible flow resonances [36] and rapid mixing. The frequency of periodic flows of the fluid is assumed to be determined by and therefore similar to that of the membrane oscillation.

In this work, we explore a more direct means to track the mixing progress, namely by the use of concentration distribution-tracking of a two-phase fluid system. A quantity describing the relative concentration of each of the two fluid phases is stored in a matrix for all cells of the mesh. A finite volume method is used, where the sum of influx and out-flux confluent on a particular elemental volume at every time-step, with respect to the adjacent cells, is used to update the relative concentration or fill-factor of each of the fluid phases in that elemental volume.

$$C_0^{n+1} = \frac{1}{\Omega}\sum_{j=1}^{6} S_j \, \Delta t\left(u_j^{in} C_j^n - u_j^{out} C_0^n\right) \qquad (10)$$

where

C_0^{n+1}, C_0^n: New and current concentration of solute in the lattice cell volume under consideration

C_j^n: Current concentration of solute in each of 6 immediate lattice cell neighbors

Ω: Volume of each lattice cell

u_j^{in}, u_j^{out}: current incoming and outing fluid velocities normal to the faces of immediate lattice cell neighbors

S_j: Surface area of one face of lattice cell

Δt: time step of current iteration

The standard deviation of the solute concentration, in all the lattice cells of the mixing chamber, is then computed and used as a measure of the mixing progress, as follows:

$$\sigma = \sqrt{\frac{1}{N}\sum_{n=1}^{N}(C_n - \langle C \rangle)^2} \qquad (11)$$

where

σ: the standard deviation of solute concentration

N: the total number of lattice cells

C_n: the solute concentration in each lattice cell at a particular time

<C>: the average solute concentration among all cells, at a particular time

A smaller standard deviation of solute concentration indicates better mixing.

5. Membrane deflection measurements

The mixing chambers were placed individually on top of an electromagnet capable of producing a maximum magnetic flux density of about 45 mT. To ensure consistency in experimentation, a 2 mm thick plastic spacer was placed in between the mixing chamber and the electromagnet. Figure 4 shows a mixing chamber placed under a top-down microscope and above the electromagnetic for a static deflection measurement. By re-focusing the microscope on the magnetic membrane under various magnetic flux densities, the vertical deflections are measured and recorded.

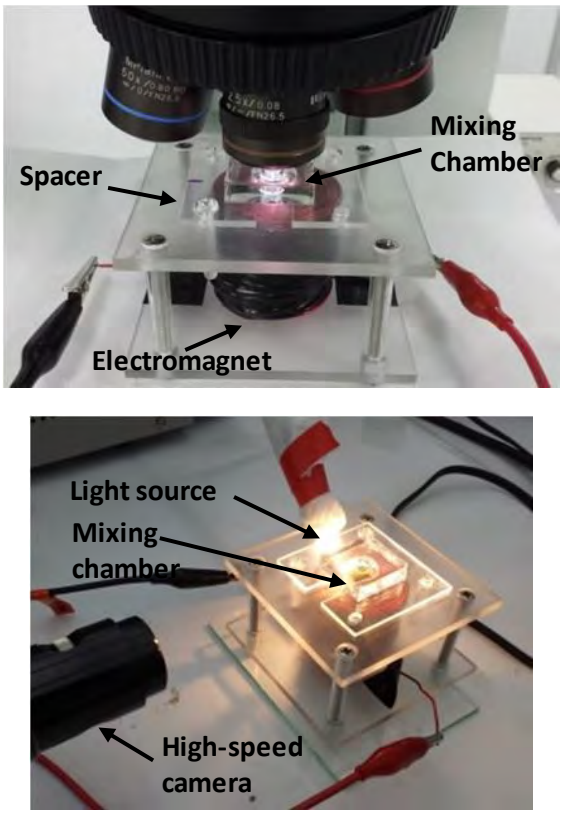

FIG.4. Mixing chamber placed between a microscope and the electromagnet (Top).High speed camera setup, where camera is pointed to the side of the chamber (Bottom).

Under a positive current input to the electromagnet, the magnetic core with positive polarity experienced a repulsive force to produce an upward membrane deflection, and vice versa. Figure 5 shows the static deflection results for the three types of design where each curve consists of three repeated measurements.

Figure 5(a) consists of results from two concentric mixers with opposing polarities. An increasing positive current will result in an upward deflection for the positive polarity mixer and a downward deflection for the negative polarity mixer. The trend is linear with a total deflection (under a current from -2.4 to 2.4 A) of ~ 228 μm for the positive polarity mixer and ~ 218 μm for the negative polarity mixer.

Figure 5(b) shows the deflection versus input current for an eccentric mixer which is also linear but exhibits a higher total deflection of ~ 389 μm when compared to the concentric mixers under the same range of current input, representing a ~ 71 % increase. Interestingly, the shifting of the magnetic core off-center results in a higher total deflection.

Figure 5(c) shows the deflection for the split mixer where one set of data represents deflection at the positive polarity region and the other set the negative polarity region. The deflections against current for both regions are linear. At each current setting of the electromagnet, the two regions will experience opposing deflections because one would be experiencing an attractive force while the other will be experiencing a repulsive force. The total deflection averages at ~121 μm which is the lowest among the three mixers and is a ~ 47 % decrease from the concentric mixer. The splitting of the magnetic core, into two opposing halves, plays a role in the reduction of the deflection. In addition to the static deflection measurements, we had also conducted dynamic deflection measurements using a high speed camera (Photron, Fastcam APX RS) setup as shown in

Figure 4. The mixing chamber was placed on top of the electromagnet and a high speed camera captured the video (at 1000 fps) of the chamber from the side during membrane actuation in which the polarity of the current to the electromagnet was switched at 100 Hz using a square waveform. Three conditions were tested: a) empty chamber (air) (Viscosity 18.7×10^{-6} Pas) [16], b) water (Viscosity 10^{-3} Pas) [17] in the chamber and c) glycerol (Viscosity of 1.412 Pas) [18] (Ajax Finechem 242) in the chamber and the results shown in Figure 6. When water was added to chamber for the three designs, the deflection values dropped significantly when compared to an empty chamber.

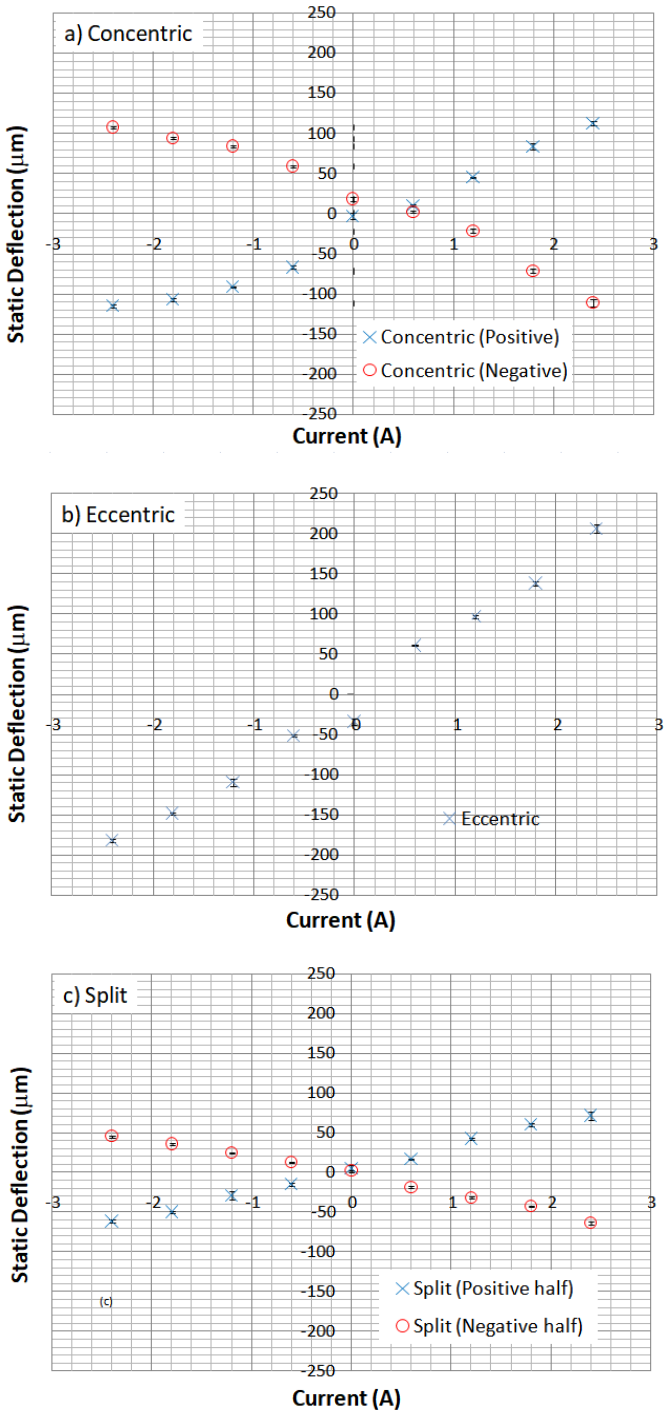

FIG. 5. Static membrane deflections for (from top to bottom): (a) concentric, (b) eccentric and (c) split type mixer designs (each graph shows the averages and standard deviations about each data point)

Glycerol, being more viscous and denser than water, had the strongest damping effect on the membrane and reduced the deflection further. The deflection performance among the three mixers was similar to what was observed in the static deflection measurements where the eccentric mixer is the highest and the split type the lowest.

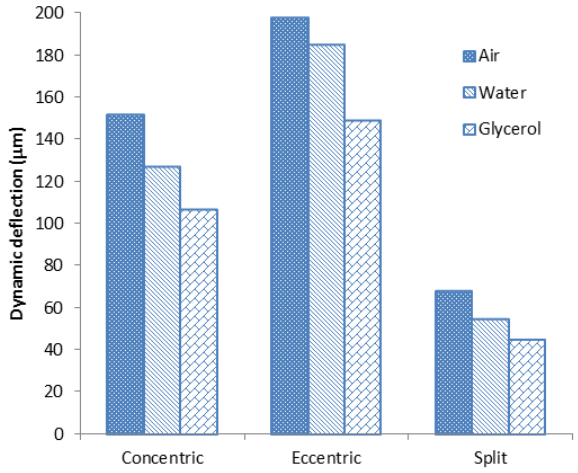

FIG. 6. Dynamic deflections of membranes under different fluids.

6. Simulation of membrane deflection

The static deflection of membranes was simulated with ANSYS Workbench to understand the membranes' behavior under actuation. As the experiment involved an electromagnet, the magnetic flux density induced was converted to pressure force by the formula:

$$F = \frac{B^2 A}{2\mu_0} \qquad (12)$$

$$P = \frac{F}{A} \qquad (13)$$

where

B is the flux density,

A is the area and

μ_0 is the permeability of vacuum ($4\pi \times 10^{-7}$).

With reference to the electromagnet's characterization, the magnetic flux density at various current inputs was expressed as pressure loadings as shown in Table 1.

TABLE I. Conversion of current to magnetic flux density and pressure loading.

Current (A)	Flux Density (mT)	Pressure (Pa)
0.6	11.2	50
1.2	19.3	148
1.8	24.9	246
2.4	28.6	325
3.0	31.1	385

In the simulation, a fixed support was applied on the model's circumference at 6 mm diameter, along with the converted pressure load applied on the magnetic core surface to produce a deflection. Meshing of the membrane model was done with medium sizing with the membrane model having 5806 nodes and 2813 elements. The following boundary conditions and assumptions were made to simulate the membrane deflection: (a) all degrees of freedom constrained on the membrane model's circumference with fixed support; (b) a uniformly-distributed pressure load applied on the magnetic core surface.

The results showed that the membrane with magnet embedded concentrically had a maximum upward deflection of 124 μm across the surface at 325 Pa. Based on eccentric design's simulated result, the magnetic core was deflected at different height at various positions. The portion of the magnetic core nearest to the edge of the membrane deflected the least while the other portion of it achieved a maximum deflection, peaking at 223 μm (representing ~ 80 % increase over the concentric design).

The split design achieved a maximum total deflection of 46 μm from both positive and negative polarity regions; a decrease of 63% from the concentric design. The result showed that one half of the magnetic core deflected upwards, while the other half deflected downwards. This was due to the nature of the magnetic sheet polarity; one being negative and the other being positive. In general, the simulation results agree with the deflection measurements in terms of relative performances and the shape of membrane profiles created were similar.

7. Results of numerical simulations of fluid flow

For the following simulations, for the purpose of comparison, all the mixers have membranes that are perturbed by the same maximum magnitude of deflection – 120 μm – in one direction from the equilibrium. However, due to the difference in the locations of the magnet on the flexible membrane in the three mixers, the membrane deformation and as-generated Gaussian pressure profile for the mixers will be different – half maximum widths of 3 mm for the Concentric, 2.1 mm for the Eccentric, and 1.5 mm for the Split mixers. The SIMPLE (Semi-Implicit Method for Pressure-Linked Equations) scheme [21] is implemented, where the pressure field is solved globally by the implicit method, after the pressures at the boundaries are updated at each time step explicitly, using the finite volume and mass residual relaxation methods. To improve convergence of the solutions, a 4th order spatial derivative-based artificial viscosity [37] is included in the viscous terms of the full Navier Stokes Equations. The non-linear advection terms are solved explicitly.

The visualizations of the pressure fields (Figures 7) and velocity fields with streamlines (Figures 8 to 10), are presented to illustrate the degree of folding that may occur for the three different mixers. Each cycle of the magnetic membrane perturbation takes 0.01 s, based on a frequency of 100

Hz. Although an adaptive time-stepping is used, to ensure accuracy, the size of the maximum time-step is limited to 10^{-4} s, so that a sample rate of at least 100 data points is possible in each cycle of membrane oscillation.

The pressure gradient varies more steeply, vertically, in the case of the concentric and eccentric mixers, compared with the split mixer. The complementary motion of the two magnets in opposite directions may have led to the gentler vertical pressure gradient, since the mass transfer in the two directions in the two halves of the chamber compensate each other. It can also be seen that both eccentric and split mixers can generate flow fields with more folding in the streamlines, due to the asymmetry of the pressure field with respect to the geometry of the mixing chamber. The eccentric mixer is able to generate tight vortices in the XZ plane, while the split mixer generates a pair of X-vortices in the YZ plane at mid vertical level position of the chamber. In addition, there is a greater transport of fluid in the lateral direction (along the axial plane of the chamber), as indicated by the streamlines in the XY view (Figure 8) and XZ view (Figure 10), which contributes to the periodic folding of the fluid interfaces. Hence, this leads to faster active mixing in the split mixer.

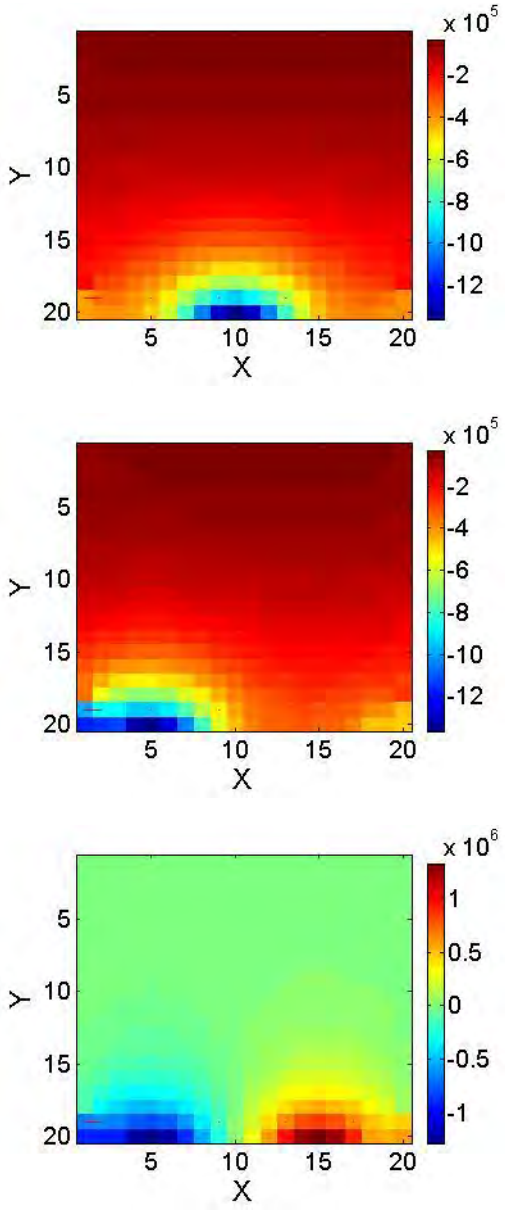

FIG. 7. Pressure Field in XY view of (top to bottom) Concentric, Eccentric, Split mixers at 0.007 s (1.4 π of cycle)

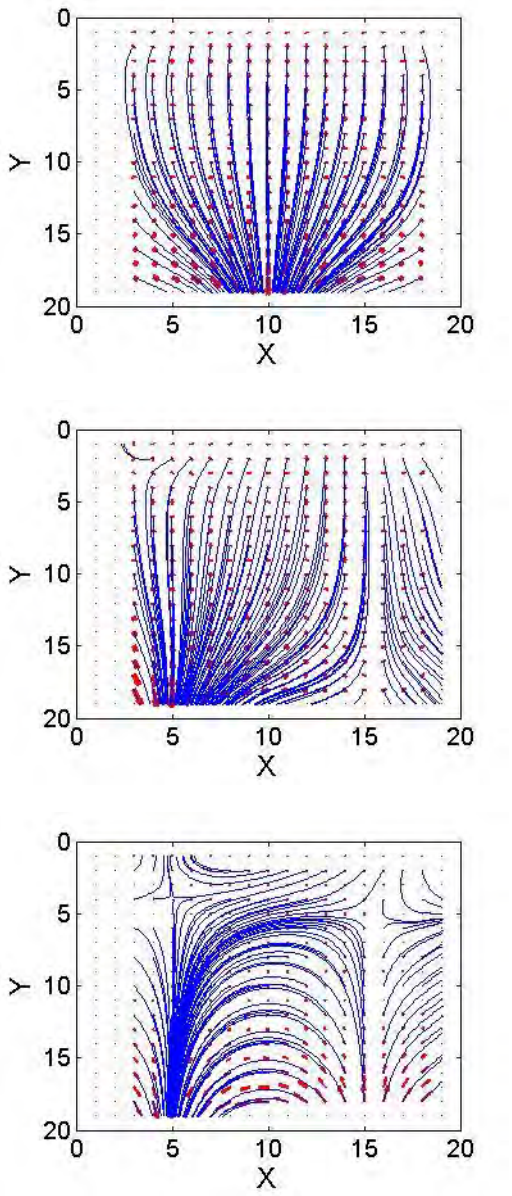

FIG. 8. Velocity Field in XY view of (top to bottom) Concentric, Eccentric, Split mixers at 0.007 s (1.4 π of cycle)

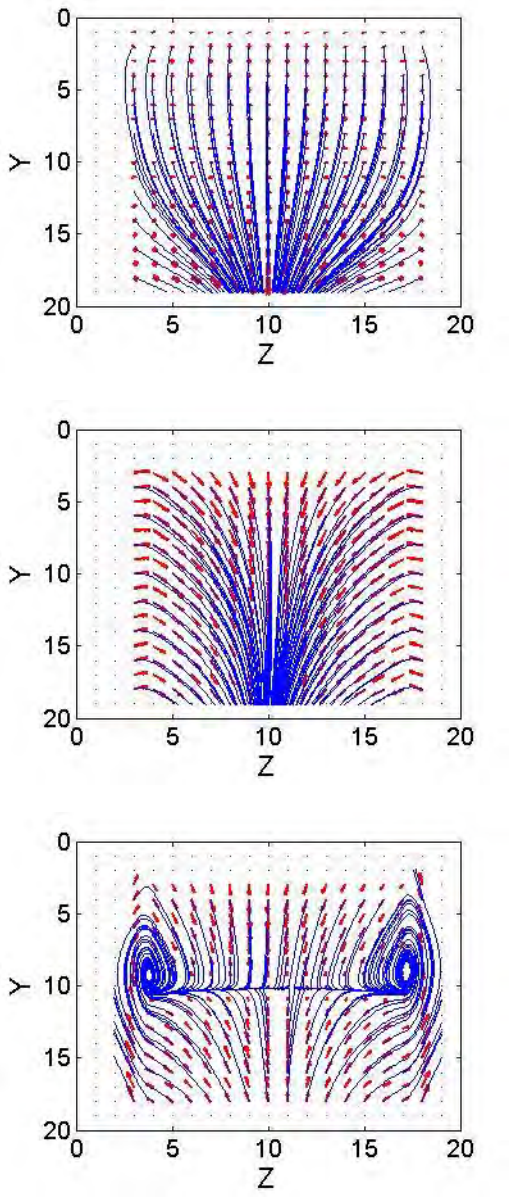

FIG. 9. Velocity Field in YZ view of (top to bottom) Concentric, Eccentric, Split mixers at 0.007 s (1.4 π of cycle)

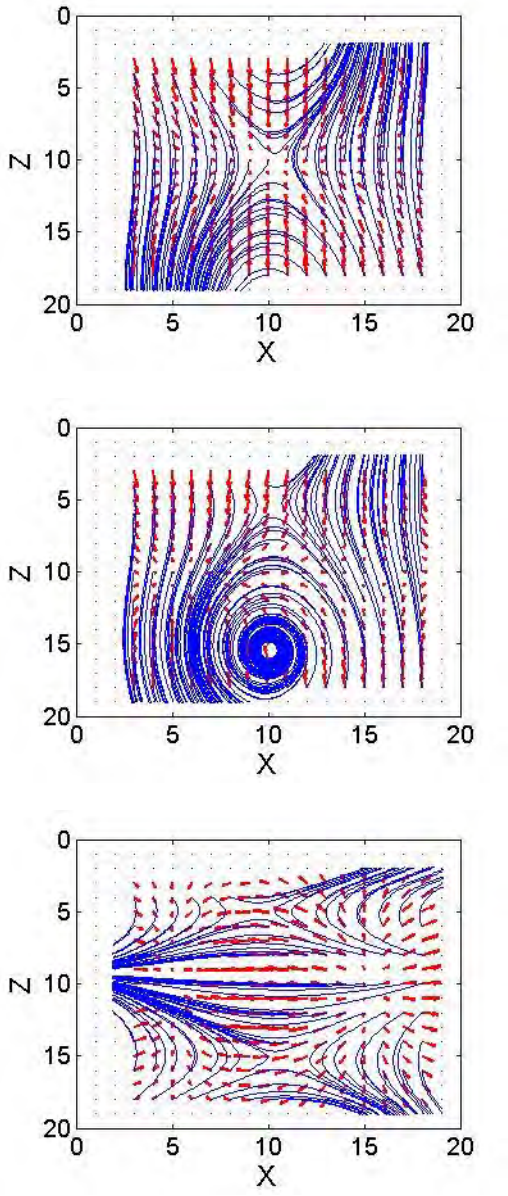

FIG. 10. Velocity Field in XZ view of (top to bottom) Concentric, Eccentric, Split mixers at 0.007 s (1.4 π of cycle)

Further on, a plot of the change in solute concentration standard deviation (Figure 11) at a particular point in time (at 30 ms from start of membrane actuation, where the standard deviation of solute concentration is reaching equilibrium), against deflection magnitudes and width of membrane deflection profile, is used for performance comparison among the three mixers. Due to the asymmetric positioning of the magnet in the eccentric mixer, the membrane assumes a skewed profile under the effects of the magnetic field, such that the pressure field generated on the fluid assumes a Gaussian profile with a narrower width (represented by the two times the standard deviation of the Gaussian curve - between 2 to 3 mm). In the split-mixer, the dual magnets of opposite polarities are located side by side, resulting in competitive dynamics of the magnets when they move in opposite directions in the applied uniform magnetic field. The forces on the magnets interact and restrict the overall deflection in either direction, such that the maximum deflection magnitude in one direction is smallest among the three mixers (about 46 um), while the profile takes on a width of

about 1.5 mm for each magnet (one half of original 3 mm-diameter round magnet). However, the solute concentration standard deviations for the split-mixer decrease at a faster rate than those of the other two mixers. This shows that even though the magnitudes of fluid flow may be lower in the split mixer, the profile of the pressure field and the locations of the magnets are important factors for realizing a faster mixing rate of the solutes, via effective folding of the phase-to-phase interface. Taking the numerical results for the decrease in solute standard deviations at 30 ms (Figure 11), where equilibrium is reached, the target design parameters used in the experimental devices (3mm width, 120 um deflection for the concentric mixer, 2.1 mm width, 220 um deflection for the eccentric mixer, and 1.5 mm width, 46 um deflection for the split mixer), the split mixer has the greatest decrease in normalized solute concentration standard deviation (0.68), followed by the eccentric (0.56) and concentric mixers (about 0.44). From the above results, it can be deduced that there is a 35 %, and 21 % time reduction for maximum degree of mixing to occur in the split and eccentric mixers respectively, in comparison with the concentric mixer. The numerical results show good agreement with the experimental results (Figures 13), with an error of 15 % for the split mixer and 5 % for the eccentric mixers, in terms of improvement in mixing rates.

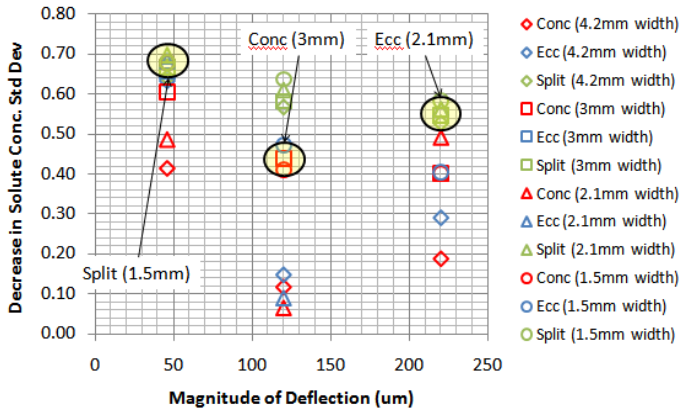

FIG. 11. Comparison of numerically computed decrease in solute concentration deviations (at 30 ms) in three mixers, with different deflection magnitudes and profile widths. Circled points are the experimental focus.

The positions of the maximum deflection of the membrane also have an effect on the mixing rate, for all three mixer types. When the two maximally deflected regions of the split mixer are shifted closer to the edge of the mixing chamber, there is a 0.2 % increase in the mixing rate (in terms of rate of solute concentration standard deviation decrease).

8. Experimental results of mixing tests

Mixing tests were conducted with the use of a high speed camera setup shown earlier in Figure 6 to capture the progression of the mixing process. 60 µL water was first loaded into the chamber, followed by the addition of 20 µL fluorescent dye (Polysciences Inc. Cat #15702). A current with square wave frequency of 100Hz was supplied to the electromagnet to generate an alternating magnetic field of ~45mT to oscillate the magnetic membrane. The energy of this oscillation would be transmitted to the fluid in the chamber creating a mixing effect. Figure 13 shows typical snapshots of the video at various times. The fluorescence dye can be seen as a bright strand suspended in water, in Fig. 13(a) just before actuation of the membrane. At the end of the mixing as shown in Fig. 13(d), the entire chamber looks homogeneous in terms of the color intensity.

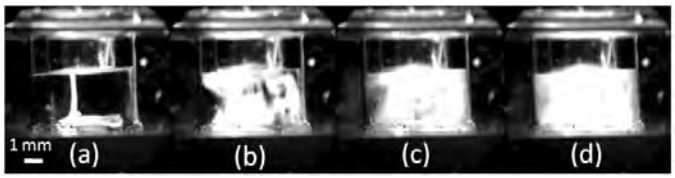

FIG. 12. Mixing of fluorescent dye in chamber with membrane actuation at (a) 0 s, (b) 2 s, (c) 4 s, (d) 8 s after addition of dye. Diameter of chamber is 6mm.

In processing the video images, the difference in intensity of pixels at each time-step was measured in the region of interest, giving a standard deviation value. These standard deviation values were used to relate to the degree of mixing, φ, based on the following formula:

$$\phi = \frac{\sigma_i - \sigma}{\sigma_i - \sigma_f} \qquad (14)$$

where

σ_i: the initial standard deviation of the grey-scale values in the region of interest.

σ_f: the final value for complete mixing, and σ, the standard deviation at a particular time-step.

Figure 13 (left graph) shows the degree of mixing against time for the three mixers with each plot being the average of five repeated mixing tests. The plots for eccentric and split designs began to reach a plateau at seven seconds where there were little changes in the pixels' intensity. For the concentric design, a steady gradient was measured and only became stable towards the end of the graph. This meant that the eccentric and split designs were able to distribute and spread the fluorescent dye around the water quicker than the concentric design, promoting more mixing within the chamber.

Even though mixing process was confirmed to be completed by magnetic membrane actuation at the end of two minutes, some values of standard deviation were still measured by the analysis software. This was due to the curvature of the circular mixing chamber. The extreme left and right sides of the mixing well appeared to be darker than the centre portion, meaning that there would still be differences in pixel intensity at steady-state; hence, the degree of mixing does not reach a perfect value of one for all mixing results.

It was expected that the eccentric design would perform better than the concentric design because the offset from center of the magnetic core resulted in a higher deflection as observed in the deflection measurements as well as in the simulation. A higher deflection would typically result in faster mixing because of the increase in fluid movement. However, the split design had similar performance as the eccentric design even though its static and dynamic deflection values were the lowest. It was initially suspected that the orientation of analysis plane may have played a part in the results obtained because the eccentric and split mixers were asymmetric. Therefore, the orientation of the high speed camera was changed to also capture the video during mixing from a second perpendicular plane.

As shown in Figure 13 (right graph), it was found out that the trend of the plots for the first and second positions behaved similarly in both the eccentric and split mixers. Slight deviations were due to the initial condition of the mixing chamber when fluorescent dye was added in. Hence, we could conclude that the orientation of analysis plane had negligible effect on the mixing efficiency results.

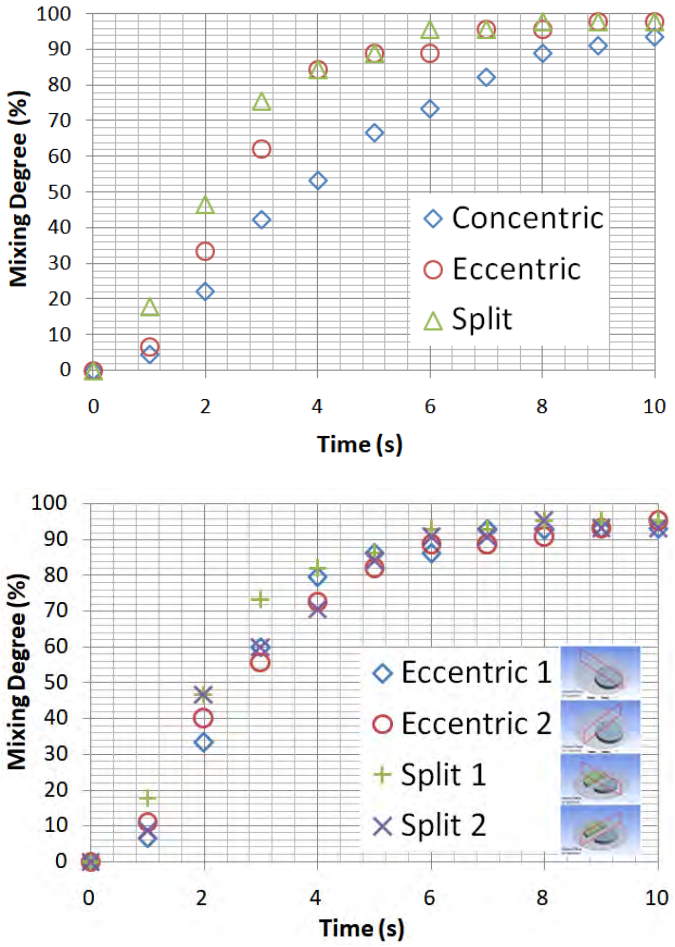

FIG. 13. Top: Degree of mixing over time for three mixers. Bottom: Mixing results for different perpendicular orientation of analysis planes-the red trapezoidal boxes in the images represent the analysis planes.

The concept of chaotic advection was demonstrated in this work. The fluorescent dye and water were able to mix quickly due to the stretching and folding of fluid lines when the membrane was actuated. The motions of fluid particles contribute to chaotic advection, the efficiency of mixing could be determined by the stretching rate of fluid lines [26], and consequently, the reduction in the diffusion paths [27].

In the case of the concentric design, the deflection profile was more uniform across the membrane which pushed the entire chamber of fluid as a bulk in the vertical plane. Mixing still occurred but some energy was spent in producing that vertical swell of fluid as we had also observed in the videos. The eccentric design had a tilted deflection profile and was able to induce vorticity in the mixing well and promote stretching of the fluid. The other reason could be that the eccentric design was able to produce a larger deflection as compared to the concentric design, creating a larger fluid movement. Even though the split design had the smallest deflection, it was compensated by its deflection profile. Under electromagnetic actuation, the two split magnetic halves of opposing polarity moved in opposite directions, causing a warping effect on the membrane which induced further instability in the motion of fluid particles in the chamber. This reciprocating, lateral twisting motion works like a "micro rocker mixer" with a more efficient transfer of energy to promote mixing by better stretching and folding of fluid lines as compared to the concentric mixer. Splitting the magnetic core into two halves of "3D" structures could also have contributed to the improved mixing.

It is observed in the video recordings of the fluid flow in mixing action during the experiments, as well as in the streamline visualizations from numerical simulations, that the fluid particles are directed in more number of folded paths which are distributed in more regions of the chamber of the split mixer, compared to the other two. This is observed to lead to faster mixing of the solute, due to the frequent and rapid transfer of material between the many vortices (large eddies, as well as micro-circulations on smaller scales) that are distributed extensively throughout the fluid volume. In the case of the other two mixers, the material trajectories over extensive regions can be seen to show more homogeneity in terms of flow orientations, and there is significant deceleration in these persistent directions due to the confinements of the chamber boundaries.

Both the eccentric and split designs were able to reduce their mixing duration by about 20-30 % as compared to that of the concentric design, indicating better efficiency. For a mixing chamber of the size presented currently in this paper (6mm in diameter), where the diffusion distance required is on the order of a millimeter, the diffusion time, and hence the typical passive mixing times would be about 10 minutes [30]. Active mixing via perturbation of a magnetic film significantly reduces the mixing times to under just 10 seconds. It was also noted that the variability during the mixing experiment for split design was lower than the eccentric design. The average variability for split design was 0.064 while eccentric design was at 0.127, which meant that the split design magnetic membrane showed a better degree of repeatability. The variability for the concentric design was 0.103.

9. Conclusion

We had designed, fabricated and characterized the performance of three micro-mixers based on flexible magnetic membrane. Computer simulation was also carried out to understand the deflection response of the membranes, as well as the resulting fluid flow due to the driving force provided by the oscillating membranes. Both experimental and numerical data showed correlated trends in mixing performances, with respect to the mixer design and its geometrical characteristics - the split mixer has a 20-30 % improvement in mixing performance, over the other two mixers. The mixing performances of the split and eccentric designs were better than the concentric mixer due to better energy transfer to promote vorticity and chaotic advection, and by imposing a strategic spatial variation of flow field by means of the split arrangements of the perturbing magnetic structures. By reconsidering the layout of magnetic core, it served as an alternative to improving mixing efficiency without the need to increase electromagnetic field strength (thereby expending more energy and generating excess heat) or using stronger magnets. Its design and construction are also sufficiently simple to facilitate integration with existing microfluidic chip designs.

Acknowledgements

This research is supported by the Singapore Institute of Manufacturing Technology (SIMTech) under the Agency for Science, Technology and Research (A*STAR) and Singapore Ministry of Education Academic Research Fund Tier 1 – RG37/15 awarded to Li King Ho Holden.

There are no conflict of interest.

References

[1] H. Becker. "IP or no IP: that is the question" Lab Chip, 2009, 23, 3327-3329

[2] Abbott, "The I-STAT System: Comprehensive Point-of-Care Testing", [Online]. Available: https://www.boundtree.com/data/default/productattachments/Abbott-Istat.pdf

[3] N.-T. Nguyen.Micromixers: Fundamentals, Design and Fabrication, 2012

[4] N.T. Nguyen and Z. Wu. "Micromixers—a review" Journal of Micromechics and Microengineering, 2005, 15, R1–R16

[5] Sobey, Ian J. (1982). "Oscillatory flows at intermediate Strouhal number in asymmetry channels" Journal of Fluid Mechanics, 125, 359–373

[6] X. Niu and Y.K. Lee. "Efficient spatial-temporal chaotic mixing in microchannels." Journal of Micromechics and Microengineering, 2003, 13, 454-462

[7] N. Pamme. "Magnetism and microfluidics" Lab Chip. 2006, 6, 24-38

[8] B. L. Gray. Journal of The Electrochemical Society, 2014, 161, B3173-B3183.

[9] M. Khoo and C. Liu. "Micro magnetic silicone elastomer membrane actuator" Sensors and Actuators A: Physical, 2001, 89, 259-266

[10] J. Li, M.Y. Zhang, L.M. Wang, W.H. Li, P. Sheng, W.J.Wen. "Design and fabrication of microfluidic mixer from carbonyl iron-PDMS composite membrane" Microfluidics and Nanofluidics, 2011, 10, 919-925

[11] H. Yu, T.B. Nguyen, S.H. Ng and T. Tran.. "Mixing control by frequency variable magnetic micropillar" Royal Society of Chemistry Advances, 2016, 6, 11822-11828.

[12] I.D. Johnston, D.K. McCluskey, C.K.L. Tan, M.C. Tracey. "Mechanical characterization of bulk Sylgard 184 for microfluidics and microengineering" Journal of Micromechics and Microengineering, 2014, 24

[13] F. Pirmoradi, L. Cheng, M. Chiao. "A magnetic poly(dimethylesiloxane) composite membrane incorporated with uniformly dispersed, coated iron oxide nanoparticles" Journal of Micromechics and Microengineering, 2010, 20

[14] Z. Z. Chong, W. J. Sim, Z. T. Yeo, K. H. Li, S. H. Ng, H. Xia, T. N. Wong, N. H. Loh, S. B. Tor, S. H. Tan, N-T Nguyen. "Elastic magnetic membrane for improved mixing in microwells" Micro and Nanosystems, 2014, 6, 232-236

[15] K. Halbach. "Design of permanent multipole magents with oriented rare earth cobalt material" Nuclear Instruments and Methods, 1980, 169,1-10.

[16] K. Kadoya, N. Matsunaga, and A. Nagashima. "Viscosity and Thermal Conductivity of Dry Air in the gaseous phase" Journal of Physical Chemistry Reference Data, 1985, 14, 4

[17] J. Kestin, M. Sokolov and W. A. Wakeham. "Viscosity of Liquid Water in the range – 8 ºC to 150 ºC" Journal of Physical Chemistry Reference Data, 1978, 7, 3

[18] J.B. Segur and H. E. Oberstar. "Viscosity of glycerol and its aqueous solutions" Industrial and Engineering Chemistry, 1951, 43, 9

[19] F. Jiang, K. S. Drese, S. Hardt, M. Kupper, and F. Schonfeld. "Helical Flows and Chaotic Mixing in Curved Micro Channels" American Institute of Chemical Engineers Journal, 2004, 50, 9

[20] O.S. Galaktionov, P.D. Anderson, G.W.M. Peters, F.N. Van de Vosse. "An adaptive front tracking technique for three dimensional transient flows" International Journal for Numerical Methods in Fluids, 2000, 32, 2, 201–217

[21] P.D. Anderson et al. "Chaotic Fluid mixing in non-quasi-static time-periodic cavity flows" International Journal of Heat and Fluid Flow, 2000, 21, 176-185

[22] P. G. M. Kruijt, O. S. Galaktionov, P. D. Anderson, G. W. M. Peters, and H. E. H. Meijer. "Analyzing Fluid Mixing in Periodic Flows by Distribution Matrices: The Mapping Method" American Institute of Chemical Engineers Journal, 2001, 47, 5, 1005-1015

[23] H.K. Moffat, A. Tsinober. "Helicity in laminar and turbulent flow" Annual Review of Fluid Mechanics, 1992, 24, 281-312

[24] H.A. Kusch, J.M. Ottino. "Experiments on mixing in continuous chaotic flows." Journal of Fluid Mechanics, 1992, 236, 319 – 348

[25] G. Metcalfe et al. "Composing Chaos: An Experimental and Numerical Study of an Open Duct Mixing Flow" American Institute of Chemical Engineers Journal, 2006, 52, 1, 9-28

[26] J. M. Ottino. The Kinematics of Mixing: Stretching, Chaos, and Transport. Cambridge University Press, 1989.

[27] J. M. Ottino. "Mixing, chaotic advection, and turbulence" Annual Review of Fluid Mechanics, 1990, 22, 207–53

[28] I. Glasgow and N. Aubry. "Enhancement of microfluidic mixing using time pulsing." Lab Chip, 2003, 3, 114–120

[29] F. Okkels and P. Tabeling. "Spatiotemporal resonances in mixing of open viscous fluids" Physical Review Letters, 2004, 92, 3.

[30] G. T. Kovacs. Micromachined Transducers Sourcebook. WCB/McGraw Hill: Boston, 1998

[31] G. G. Yaralioglu, I. O. Wygant, T. C. Marentis, and B. T. Khuri-Yakub."Ultrasonic Mixing in Microfluidic Channels Using Integrated Transducers" Analytical Chemistry, 2004, 76, 13, 3694-3698

[32] T. Nishimura and K. Kunitsugu. "Fluid mixing and mass transfer in two-dimensional cavities with time-periodic lid velocity." International Journal of Heat and Fluid Flow, 1997, 18, 5, 497-506

[33] H.M. Xia, C. Shu, S. Y. M. Wan, Y. T. Chew. "Influence of the Reynolds number on chaotic mixing in a spatially periodic micromixer and its characterization using dynamical system techniques." Journal of Micromechanics and Microengineering, 2006, 16, 53-61

[34] S. Takasaki, K. Ogawara. "A Study on Chaotic Mixing in 2D Cavity Flows: Effects of Reynolds Number and Amplitude of Lid Velocity" JSME International Journal.Series B Fluids and Thermal Engineering, 1994, 37, 2, 237-241

[35] M. Chiba, H. Watanabe, H.F. Bauer. "Hydroelastic coupled vibrations in a cylindrical container with a membrane bottom, containing liquid with surface tension." Journal of Sound and Vibration, 2002, 251, 4, 717-740

[36] M. Heil, S. L. Waters. "Transverse Flows in rapidly oscillating elastic cylindrical shells Journal of Fluid Mechanics, 2006, 547, 185–214.

[37] A.W. Cook, W.H. Cabot. "A high-wavenumber viscosity for high-resolution numerical methods." Journal of Computational Physics, 2004, 195, 594–601

[38] G.P. Celata, G.L. Morini, V. Marconi, S.J. McPhail, G. Zummo. "Using viscous heating to determine the friction factor in microchannels – An experimental validation." Experimental Thermal and Fluid Science, 2006, 30, 725–731.

[39] R H Liu et al. "Passive mixing in a three-dimensional serpentine microchannel" Journal of Microelectromechanical Systems., 2000, 9, 2, 190–197

[40] R. A. Vijiayendran et al. "Evaluation of a three-dimensional micromixer in a surface-based biosensor" Langmuir 2003, 19, 5, 1824–1828

[41] H. Chen and J. C. Meiners. "Topologic mixing on a microfluidic chip" Applied Physics Letters, 2004, 84, 2193

[42] S. J. Park et al. "Rapid three-dimensional passive rotation micromixer using the breakup process" Journal of Micromechics and Microengineering, 2003, 14, 1, 6–14

[43] Y. Du et al. "Evaluation of Floor-grooved Micromixers Using Concentration-channel Length Profiles" Micromachines, 2010, 1, 19-33.

[44] G.R. Ziegler, A. L. Benado, S. S. H. Rizvi. "Determination of Mass Diffusivity of Simple Sugars in Water by the Rotating Disk Method" Journal of Food Science, 1987, 52, 2, 501-502

Biographies

Shao Qiang Tang received a degree in Electrical and Computer Engineering from the National University of Singapore, and M.Sc. degree in Biomedical Engineering from the Nanyang Technological University. He had worked in various national institutes on sensor devices and nanomaterials synthesis, and had also joined Bayer MaterialScience as a research engineer, working on nanomaterials synthesis and polymer formulations for coating of flexible electronics. He is currently a research associate at the Nanyang Technological University, working on the analysis and simulations of microfluidics devices design.

Dr Holden King Ho Li received the B.Eng. degree from the National University of Singapore, in 1997, and the M.S. and Ph.D. degrees from Stanford University, CA, USA, in 2002 and 2005, respectively, all in mechanical engineering. In 2013, he joined the School of Mechanical and Aerospace Engineering, Nanyang Technological University, Singapore, where he currently focus on micro and nanofabrication methods and MEMS reliability study. Besides, Holden is actively working in the area of BioMEMS.

Wei Xuan Chan received his Ph.D. degree in Mechanical Engineering from Nanyang Technological University, Singapore in 2016. His current research is in micro-scaled acoustics.

Dr Say Hwa Tan is an ARC DECRA fellow with Queensland Micro-and Nanotechnology Centre, Griffith University, Australia. He received his B.Eng., M.Eng. and Ph.D. degrees from the Nanyang Technological University, Singapore, and the Georg-August-Universität Göttingen/Max Planck Institute for dynamics and self-organization (MPI-DS), Germany, in 2008, 2010 and 2014 respectively. In 2016, he was highlighted as one of the 18 emerging investigators in the journal of Lab on a Chip. Dr Tan has published more than 30 research works in microfluidics. His research has established and pioneered different approaches to manipulate droplets and bubbles using thermal, magnetic, acoustic and electric energy.

Dr Sum Huan Ng received his B.Eng. and M.Eng. in mechanical engineering in 1997 and 2000 respectively from the National University of Singapore. He obtained his Ph.D. from the Georgia Institute of Technology. He is currently a senior scientist and programme manager for microfluidics manufacturing with SIMTech working in the areas of microfluidics, lab-on-a-chip, microfabrication techniques and biosensing.